

## Article

# Modified Gold Screen-Printed Electrodes for the Determination of Heavy Metals

Consuelo Celesti <sup>1,\*</sup>, Salvatore Vincenzo Giofrè <sup>2,\*</sup>, Claudia Espro <sup>1</sup>, Laura Legnani <sup>3</sup>, Giovanni Neri <sup>1</sup>  
and Daniela Iannazzo <sup>1</sup>

<sup>1</sup> Department of Engineering, University of Messina, Contrada Di Dio, 98166 Messina, Italy; espro@unime.it (C.E.); gneri@unime.it (G.N.); diannazzo@unime.it (D.I.)

<sup>2</sup> Department of Chemical, Biological, Pharmaceutical and Environmental Sciences, University of Messina, Viale Ferdinando Stagno D'Alcontres 31, 98166 Messina, Italy

<sup>3</sup> Department of Biotechnology and Biosciences, University of Milano Bicocca, Piazza della Scienza 2, 20126 Milano, Italy; laura.legnani@unimib.it

\* Correspondence: ccelesti@unime.it (C.C.); sgiofre@unime.it (S.V.G.)

**Abstract:** Screen-printed electrodes (SPEs) are reliable, portable, affordable, and versatile electrochemical platforms for the real-time analytical monitoring of emerging analytes in the environmental, clinical, and agricultural fields. The aim of this study was to evaluate the electrochemical behavior of gold screen-printed electrodes (SPGEs) modified with molecules containing amino (**Tr-N**) or  $\alpha$ -aminophosphonate (**Tr-P**) groups for the selective and sensitive detection of the toxic metal ions  $\text{Pb}^{2+}$  and  $\text{Hg}^{2+}$  in aqueous samples. After optimizing the analytical parameters (conditioning potential and time, deposition potential and time, pH and concentration of the supporting electrolyte), anodic square wave stripping voltammetry (SWASV) was used to evaluate and compare the electrochemical performance of bare or modified electrodes for the detection of  $\text{Hg}^{2+}$  and  $\text{Pb}^{2+}$ , either alone or in their mixtures in the concentration range between 1 nM and 10 nM. A significative improvement in the detection ability of  $\text{Pb}^{2+}$  ions was recorded for the amino-functionalized gold sensor **SPGE-N**, while the presence of a phosphonate moiety in **SPGE-P** led to greater sensitivity towards  $\text{Hg}^{2+}$  ions. The developed sensors allow the detection of  $\text{Pb}^{2+}$  and  $\text{Hg}^{2+}$  with a limit of detection (LOD) of 0.41 nM and 35 pM, respectively, below the legal limits for these heavy metal ions in drinking water or food, while the sensitivity was  $5.84 \mu\text{A nM}^{-1}\text{cm}^{-2}$  and  $10 \mu\text{A nM}^{-1}\text{cm}^{-2}$ , respectively, for  $\text{Pb}^{2+}$  and  $\text{Hg}^{2+}$ . The reported results are promising for the development of advanced devices for the in situ and cost-effective monitoring of heavy metals, even in trace amounts, in water resources.

**Keywords:** heavy metals; screen-printed electrodes; electrochemical detection; anodic stripping voltammetry



**Citation:** Celesti, C.; Giofrè, S.V.; Espro, C.; Legnani, L.; Neri, G.; Iannazzo, D. Modified Gold Screen-Printed Electrodes for the Determination of Heavy Metals. *Sensors* **2024**, *24*, 4935. <https://doi.org/10.3390/s24154935>

Received: 4 July 2024

Revised: 28 July 2024

Accepted: 29 July 2024

Published: 30 July 2024



**Copyright:** © 2024 by the authors. Licensee MDPI, Basel, Switzerland. This article is an open access article distributed under the terms and conditions of the Creative Commons Attribution (CC BY) license (<https://creativecommons.org/licenses/by/4.0/>).

## 1. Introduction

With the progress of industrial development, global environmental pollution has become more critical [1–3]. Heavy metal ions are among the most relevant water contaminants affecting terrestrial and aquatic ecosystems [4,5]. The foremost source of these heavy metal ions are cosmetics and their derivatives. Another source is chemicals from industrial or domestic waste [6]. Heavy metal ions are spread everywhere and are not able to be degraded. For this reason, these pollutants pose a threat to human health and the environment [7]. These ions are released from factories, accumulate in the biosphere, and then penetrate organisms through the food chain. Heavy metals such as mercury, cadmium, arsenic, and lead represent a risk to human health even at low concentrations since they react with the thiol group of proteins and thus enter cells, altering the biochemical life cycle [8]. Furthermore, high concentrations of silver and copper also have harmful effects [7,9,10]. These metals are extremely hazardous pollutants and are among the top ten on the 'Priority List of Hazardous Substances of Toxic Substances and Disease Registry' [11–13]. Disease

Control and the European Union have listed heavy metals as priority substances and have instituted a list of permitted concentration limits [14]. The Joint Expert Committee on Food Additives of the Food and Agriculture Organization/World Health Organization and the International Agency for Research on Cancer evaluate the toxicity of heavy metals [15–17]. In recognition of the risks that heavy metal ions represent for the environment and for the human organism, it is particularly important to have an accurate and efficient detection technology. Exposure to lead and mercury specifically can cause health problems extending from stomach aches to brain damage. The U.S. Environmental Protection Agency (EPA) has set detection limits for these heavy metals, which are 15 µg/L and 0.6 µg/L for lead and mercury, respectively [18,19].

Several methods have been developed for the detection of heavy metal ions, such as atomic absorption spectroscopy [20,21], mass spectroscopy with inductively coupled plasma [22–26], neutron activation analysis [27,28], X-ray fluorescence spectrometry [29–34], and optical emission with inductively coupled plasma [23,35–38]. These technologies provide excellent detection limits and can measure several metal ions simultaneously. Nevertheless, spectroscopic techniques are expensive. Qualified staff can only use the instruments required for these techniques, involving complex pre-processing and sample analysis methods. Although optical techniques can exactly detect heavy metal ions, expensive heavy metals, pricey equipment, and complex operations are required. Additionally, these techniques are not well adapted for on-site detection [39,40]. Hence, efficient, low-cost, simple, and reliable detection technology is a crucial path to detect metal ions in situ [41–45].

Electrochemical detection can be applied to overcome the limitations of other methods. Electrochemical methods are easy to use, cheap, and reliable. In addition, these techniques can be implementable in the field, providing portability and rapid response to the on-site analysis of polluted samples. Modifying electrochemical sensors with specific substances can significantly improve their performance. For example, the loading with metal nanoparticles can accelerate the electron transfer rate between the analyte and the electrode. Semiconductor nanomaterials can enhance the efficiency of photochemical reactions and improve the detection performance of heavy metal ions [46–48]. The sensitivity and detection limit of electrochemical techniques can be improved by using several electrochemical sensors combined with different electrochemical techniques, which offer lower complexity, higher analysis speed, lower cost, and miniaturization capability with detection limits of ppb (part per billion) [49,50]. Therefore, these techniques have long been suggested as alternative strategies for the in situ monitoring of heavy metals.

Among the wide range of electrochemical techniques, anodic stripping voltammetry (ASV) has demonstrated the ability to sensitively detect most heavy metals, even in trace amounts [51]. Considering the relevance of miniaturization to improve field performance, screen-printed electrodes (SPEs) represent the key to developing new portable sensing systems in recent years. SPEs are simple, economical, very suitable for on-site analysis, and can be used to develop versatile (bio)sensors for a variety of applications, including clinical biomarkers, environmental monitoring, and agrifood sectors [51–55].

SPEs with gold working electrodes (SPGEs) are particularly suitable for a wide range of biosensing applications [56]. The easy gold surface functionalization with homobifunctional thiol-cleavable crosslinking reagents, such as the dithiobis (succinimidyl propionate linker (DSP), allows the development of self-assembled monolayers (SAMs) on the electrode surface, obtaining good reproducibility and high electron transfer rates [57].

In the present research, we wanted to investigate, for the first time, the thiol chemistry functionalization of SPGE for selective heavy metal detection. The working electrodes of SPGEs have been modified with the molecules **Tr-N** and **Tr-P** containing amino or  $\alpha$ -aminophosphonate groups, which are able to recognize  $\text{Pb}^{2+}$  and  $\text{Hg}^{2+}$ , respectively, in water. The selected ligands have previously demonstrated, through experimental and computational studies, the ability to selectively bind  $\text{Hg}^{2+}$  or  $\text{Pb}^{2+}$  ions, respectively, in mixtures of these and other competing ions [58]. These sensitive elements have been

covalently linked to the electrodes using the cross-linker dithiobis(succinimidylpropionate) (DSP), which is able to form stable Au-S bonds [59], and covalently link the sensitive elements through the two NHS-activated esters to obtain **SPGE-N** and **SPGE-P**. After the optimization of the chemical and instrumental conditions, type of supporting electrolyte, deposition potential, pH, and time, square wave stripping anodic voltammetry (SWASV) was chosen as the electrochemical method for the detection of  $\text{Hg}^{2+}$  and  $\text{Pb}^{2+}$  alone or in their mixtures. **SPGE-N** and **SPGE-P** demonstrated a good selectivity towards  $\text{Pb}^{2+}$  and  $\text{Hg}^{2+}$  ions, respectively, with a limit of detection of 0.41 nM for  $\text{Pb}^{2+}$  and 35 pM for  $\text{Hg}^{2+}$ , which are below the legal limits in drinking water or food. The obtained results, compared with those obtained from bare gold electrodes, highlight the improved selectivity and sensitivity of the modified sensors towards the selected toxic ions. This study can pave the way for an innovative, reliable, and, at the same time, accessible route for monitoring water quality using simply modified SPEs and anodic stripping voltammetry.

## 2. Materials and Methods

### 2.1. Chemicals and Materials

All reagents and solvents were acquired from Sigma Aldrich (St. Louis, MO, USA) and used without any further purification. Lead nitrate (purity  $\geq 99.95\%$ ) and mercury nitrate monohydrate (purity  $\geq 99.99\%$ ) were used to prepare aqueous solutions of the heavy metals concerned. The acetate buffer was prepared using a 0.1 M solution of acetic acid and NaOH to obtain the desired pH. Double-distilled water was used for the entire experimental part. All chemicals and reagents were of analytical grade and were used without additional purification, unless otherwise stated. SPGEs were purchased from Metrohm-DropSens ([www.dropsens.com](http://www.dropsens.com)). NMR spectra were recorded at 500 MHz; chemical shifts are given in parts per million, using trimethylsilane (TMS) as the internal standard. Thin-layer chromatography was performed on aluminum plates pre-coated with Merck 60-F254 silica gel. Preparative separations were carried out by flash column chromatography using 0.063–0.200 mm Merck silica gel. Infrared spectra were obtained with a Spectrum Two FT-IR spectrometer (PerkinElmer Inc., Waltham, MA, USA) using the ATR method in the range 4000–500  $\text{cm}^{-1}$ . The percentage of elemental composition (including carbon, nitrogen, hydrogen, sulfur, and oxygen) in the samples was also determined with the CHNS-O EMA 502 VELD (NY, USA).

### 2.2. Synthesis of the Sensitive Elements **Tr-N** and **Tr-P**

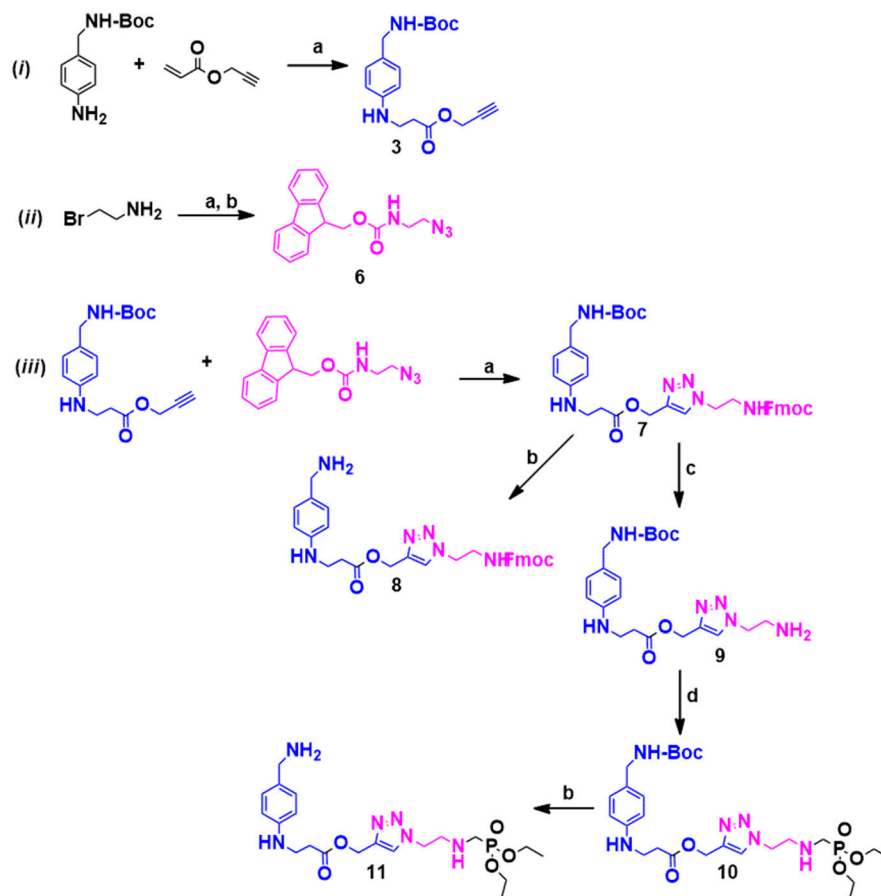
#### 2.2.1. Synthesis of **Tr-N**

As depicted in Scheme 1, the synthesis of **Tr-N** involved the click chemistry reaction of prop-2-yn-1-yl-3-((4-(((tert-butoxycarbonyl)amino)methyl)phenyl)amino) propanoate **3**, obtained from the Michael-type reaction of **1** and **2**, with (9H-fluoren-9-yl)methyl (2-azidoethyl)carbamate **5**, derived from 2-bromoethylamine **4**, and the subsequent Boc-deprotection, following the procedure reported below.

Synthesis of prop-2-yn-1-yl 3-((4-(((tert-butoxycarbonyl)amino)methyl)phenyl)amino) propanoate (**3**). To a solution of tert-butyl 4-aminobenzylcarbamate **1** (1 g, 4.50 mmol) in HFIP (10 mL), we added propargyl acrylate **2** (1 mL, 9 mmol) at r.t. The reaction was allowed to react at room temperature for 48 h. After this time, the solvent was removed under reduced pressure and the residue was purified by flash chromatography on silica gel ( $\text{CHCl}_3/\text{MeOH}$  95:5) to obtain the pure product **3** as a yellow solid (see Supplementary Materials for NMR data and elemental analyses).

Synthesis of (9H-fluoren-9-yl)methyl (2-azidoethyl)carbamate (**5**). 2-Bromoethylamine **4** (6.161 g, 30 mmol) was added to a solution of sodium azide (6.20, 95 mmol) in 20 mL of distilled water. The reaction was conducted under reflux at 80 °C for 24 h. The reaction mixture was cooled to 0 °C, and KOH (7.99 g, 142 mmol) was added. The reaction was allowed to react at 0 °C and was extracted with ethyl acetate (4 × 35). To a suspension of fluorenylmethoxycarbonyl chloride (1531 g, 5.92 mmol) in acetone (20 mL), a solution of 2-azido-ethylamine (509 mg, 5.92 mmol) and potassium carbonate (818 mg, 5.92 mmol) was

added in 15 mL of distilled water. The reaction was allowed to react overnight at room temperature. After this time, the solvent was removed under reduced pressure, and the residue was first extracted with ethyl acetate (4 × 50) and then purified by flash chromatography on silica gel (CHCl<sub>3</sub>/MeOH 95:5) to obtain **5** as a white solid (see Supplementary Materials for NMR data and elemental analyses).



**Scheme 1.** Reagents and conditions: (i) (a) HFIP, 48 h at r.t., yield 90%; (ii) (a) NaN<sub>3</sub>, H<sub>2</sub>O, 80 °C, 24 h, yield 88%; (b) Fmoc-Cl, KOH, Acetone, 12 h, t.a. yield 85%; (iii) (a) CuSO<sub>4</sub>·5H<sub>2</sub>O, sodium ascorbate, TEA, 12 h, t.a., yield 85%; (b) trifluoroacetic acid, DCM, 1h, t.a., yield 80%, (c) piperidine, CH<sub>2</sub>Cl<sub>2</sub>, overnight, yield 90%; (d) CH<sub>2</sub>O (37 wt%), triethyl phosphite, 16 h, reflux, yield 60%.

Synthesis of (1-(2-(((9H-fluoren-9-yl)methoxy)carbonyl)amino)ethyl)-1H-1,2,3-triazol-4-yl)methyl 3-((4-(((tert-butoxycarbonyl)amino)methyl)phenyl)amino)propanoate (**6**). To a dispersion of ethynyl 2-((4-(((tert-butoxycarbonyl)amino)methyl)phenyl)amino)acetate **3** (181 mg, 0.54 mmol), (9H-fluoren-9-yl)methyl (2-azidoethyl)carbamate **5** (168 mg, 0.54 mmol), and triethylamine (0.08 mL, 0.54 mmol) in acetonitrile (20 mL) and distilled water (20 mL), copper sulfate (34 mg, 0.135 mmol) and sodium ascorbate (53.49 mg, 0.27 mmol) were added. The reaction is left under stirring overnight at room temperature. After this time, the solvent was removed under reduced pressure, and the residue was purified by flash chromatography on silica gel (CHCl<sub>3</sub>/MeOH 95:5) to obtain the pure product **6** as a yellow oil (see Supplementary Materials for NMR data and elemental analyses).

Synthesis of (1-(2-(((9H-fluoren-9-yl)methoxy)carbonyl)amino)ethyl)-1H-1,2,3-triazol-4-yl)methyl 3-((4-(aminomethyl)phenyl)amino)propanoate (**Tr-N**). To a solution of (1-(2-(((9H-fluoren-9-yl)methoxy)carbonyl)amino)ethyl)-1H-1,2,3-triazol-4-yl)methyl 3-((4-(((tert-butoxycarbonyl)amino)methyl)-phenyl)amino)-propanoate **6** (450 mg, 0.7 mmol) in CH<sub>2</sub>Cl<sub>2</sub> (30 mL), trifluoroacetic acid (1.07 mL, 14 mmol) was added, and the mixture was allowed to react at room temperature overnight. After this time, the mixture was extracted with CH<sub>2</sub>Cl<sub>2</sub> (4 × 40) and was purified by flash chromatography

on silica gel (CHCl<sub>3</sub>/MeOH 95:5) to obtain the pure product **Tr-N** as a yellow oil (see Supplementary Materials for NMR data and elemental analyses).

### 2.2.2. Synthesis of **Tr-P**

The synthesis of **Tr-P** was performed, starting from compound **6** by Fmoc-deprotection, a subsequent Mannich-type reaction of the free amino group with formaldehyde and triethyl phosphite, and finally by the cleavage of the Boc group. Below, the detailed procedure is reported.

Synthesis of (1-(2-aminoethyl)-1H-1,2,3-triazol-4-yl)methyl 3-((4-(((tert-butoxycarbonyl)amino) methyl)phenyl)amino)propanoate (**7**). To a solution of (1-(2-(((9H-fluoren-9-yl) methoxy)carbonyl)amino)ethyl)-1H-1,2,3-triazol-4-yl)methyl 3-((4-(((tert-butoxycarbonyl) amino)methyl)-phenyl)amino)-propanoate **6** (778 mg, 1.214 mmol) in CH<sub>2</sub>Cl<sub>2</sub> (30 mL), piperidine (0.07 mL, 1.214 mmol) was added, and the mixture was allowed to react at room temperature overnight. After this time, the solvent was removed under reduced pressure and the residue was purified by flash chromatography on silica gel (CHCl<sub>3</sub>/MeOH 9:1) to obtain the pure product **7** as a yellow oil (see Supplementary Materials for NMR data and elemental analyses).

Synthesis of (1-(2-(((diethoxyphosphoryl)methyl)amino)ethyl)-1H-1,2,3-triazol-4-yl) methyl 3-((4-(((tert-butoxycarbonyl)amino)methyl)phenyl)amino)propanoate (**8**). To a solution of (1-(2-aminoethyl)-1H-1,2,3-triazol-4-yl)methyl 3-((4-(((tert-butoxycarbonyl)amino) methyl)phenyl)amino)propanoate **7** (210 mg, 0.5 mmol) in ethanol (3 mL), triethyl phosphite (0.125 mmol, 0.022 mL) and formaldehyde solution 37% (0.25 mmol, 0.02 mL) was added, and the mixture was allowed to react at reflux for 16 h. After this time, the solvent was removed under reduced pressure and the residue was purified by flash chromatography on silica gel (CHCl<sub>3</sub>/MeOH 95:5) to obtain the pure product **8** as a yellow oil (see Supplementary Materials for NMR data and elemental analyses).

Synthesis of (1-(2-(((diethoxyphosphoryl)methyl)amino)ethyl)-1H-1,2,3-triazol-4-yl)methyl 3-((4-(aminomethyl)phenyl)amino)propanoate (**Tr-P**). To a solution of (1-(2-(((diethoxyphosphoryl) methyl)amino)ethyl)-1H-1,2,3-triazol-4-yl)methyl 3-((4-(((tert-butoxycarbonyl)amino)methyl) phenyl)amino)propanoate **8** (100 mg, 0.176 mmol) in CH<sub>2</sub>Cl<sub>2</sub> (10 mL), trifluoroacetic acid (0.29 mL, 3.517 mmol) was added, and the mixture was allowed to react at room temperature overnight. After this time, the volatiles were removed in vacuo. The crude was diluted with CH<sub>2</sub>Cl<sub>2</sub> and sat. aq. NaHCO<sub>3</sub>. The mixture was extracted with CH<sub>2</sub>Cl<sub>2</sub> (4 × 30) and was purified by flash chromatography on silica gel (CHCl<sub>3</sub>/MeOH 9:1) to obtain the pure product **Tr-P** as a yellow oil (see Supplementary Materials for NMR data and elemental analyses).

### 2.3. Development of the Modified SPGEs (**SPGE-N** and **SPGE-P**)

To develop the **SPGE-N** and **SPGE-P** electrodes, the bare SPGEs were first functionalized using the reagent DSP as follows. A quantity of 10 mg of DSP was ultrasonically dissolved in 1 mL of DMSO. Then, 15 µL of the solution was dropped directly onto the surface of the gold working electrode and allowed to dry at room temperature until further use. Next, 10 mg of **Tr-N** or **Tr-P** was dissolved in 1 mL of DMSO. Then, 20 µL of the two solutions were deposited directly onto the surface of the DSP-SPGE gold working electrodes to obtain **SPGE-N** and **SPGE-P**, which were left to dry at room temperature until further use.

### 2.4. Electrochemical Tests

Electrochemical investigations were performed in a 5 mL beaker using the DropSens µStat 400 potentiostat and Dropview version 8400 software for data acquisition. Important instrumental parameters for SWV, such as the conditioning potential/time (Econd/tcond) and deposition potential/time (Edep/tdep), were each optimized and found to be 0.6 V/60 s and 1.1 V/240 s, respectively. After the pre-concentration step, analyses were carried out ranging from −1.1 to 0.8 V to achieve the analytical signal for the heavy metal concentration

and subsequently to construct the calibration curves for each analyte. Initially, the response of the modified electrode without the presence of the ions was recorded. A stirring speed of 300 rpm was applied for the deposition of the ions prior to measurement. SWV was performed by adding microvolumes of standard aqueous solutions of metal ions to the electrochemical cell containing 5 mL of acetate buffer solution. To stabilize the SPEs, triplicate scans were performed for each new unit in the buffer solution before reliable measurements were made. To ensure the removal of metal ions from the working surface of the SPEs, a conditioning potential was applied at  $-1$  V for 60 s before each measurement.

### 3. Results and Discussion

#### 3.1. Synthesis of Tr-N and Tr-P

The synthetic strategy for the development of the sensitive elements **Tr-N** and **Tr-P** to be loaded on the working electrode of SPGEs involves, as a key step, the formation of the 1,4-disubstituted-1,2,3-triazole **6** by Huisgen 1,3-dipolar cycloaddition reaction of the propargyl derivative **3** and azide **5**, as depicted in Scheme 1 [60,61]. Compound **3** was obtained by a Michael-type addition reaction between the free amino group of tert-butyl 4-aminobenzylcarbamate **1** and the terminal double bond present in propargyl acrylate **2** (path *i*), while the reaction of 2-bromoethylamine **4** with sodium azide followed by the protection of the free amino group with fluorenylmethoxycarbonyl chloride (Fmoc) provided azide **5** (path *ii*). The Cu(II)-catalyzed 1,3-dipolar cycloaddition of **3** and **5**, performed in the presence of ascorbate and in mild reaction conditions, afforded the triazole derivative **6** in a nearly quantitative yield (path *iii*). The sample **Tr-N** was then obtained in a quantitative yield by the deprotection of the Boc group using TFA at room temperature. For the synthesis of the **Tr-P** sample, the cleavage of Fmoc in compound **6** allowed the Mannich-type reaction of the free amino functionality of compound **7** with formaldehyde and triethyl phosphite to obtain compound **8**. Finally, the cleavage of the Boc group performed again using TFA afforded the **Tr-P** sample. All the synthesized compounds and intermediates have been purified and characterized, as reported in the experimental section.

#### 3.2. Synthesis of the Ligand-Modified SPGE

The bare SPGEs were easily functionalized using the Lomant's reagent as follows to obtain **SPGE-N** and **SPGE-P** electrodes, respectively (Figure 1). A quantity of 10 mg DSP (Lomant's reagent) was ultrasonically dissolved in 1 mL of DMSO. Then, 15  $\mu$ L of the solution was dropped directly onto the surface of the gold working electrode and allowed to dry at room temperature until further use. Next, 10 mg of samples **8** and **9** were dissolved in 1 mL of DMSO, respectively. Then, 20  $\mu$ L of the two solutions were deposited directly onto the surfaces of the gold working electrodes (SPGEs) previously modified with DSP and left to dry at room temperature until further use.

The Fourier transform infrared spectroscopy was used to verify the effectiveness of the chemical modification on the work electrode of SPGE. As shown in Figure 2, the FTIR spectra of SPGE showed no peaks. After modification with DSP, the absorbance peaks shown in the SPGE-DSP spectrum at  $1786\text{ cm}^{-1}$  and  $1740\text{ cm}^{-1}$  indicate the representative symmetric and asymmetric carbonyl stretches (respectively) of the NHS ester. Furthermore, the peak at  $1212\text{ cm}^{-1}$  confirms the presence of the asymmetrical C-N-C stretch of the NHS ester, while the peak at  $1069\text{ cm}^{-1}$  can be identified as the N-C-O stretch of succinimide. Finally, the peak at  $1170\text{ cm}^{-1}$  indicates the carbonyl stretch of the ester. The presence of these peaks confirms the chemisorption of DSP on the gold surface. The electrode modification with DSP significantly changed the IR spectrum of the gold substrate; this sample shows the diagnostic peak at  $1680\text{ cm}^{-1}$  due to the carbonyl stretch of amide moiety. The spectrum of **SPGE-N** shows the representative absorbance of the triazole ring at  $1440\text{ cm}^{-1}$  due to the N=N stretching, while, for **SPGE-P**, the diagnostic peak at  $1024\text{ cm}^{-1}$  due to the P=O stretching can be observed.

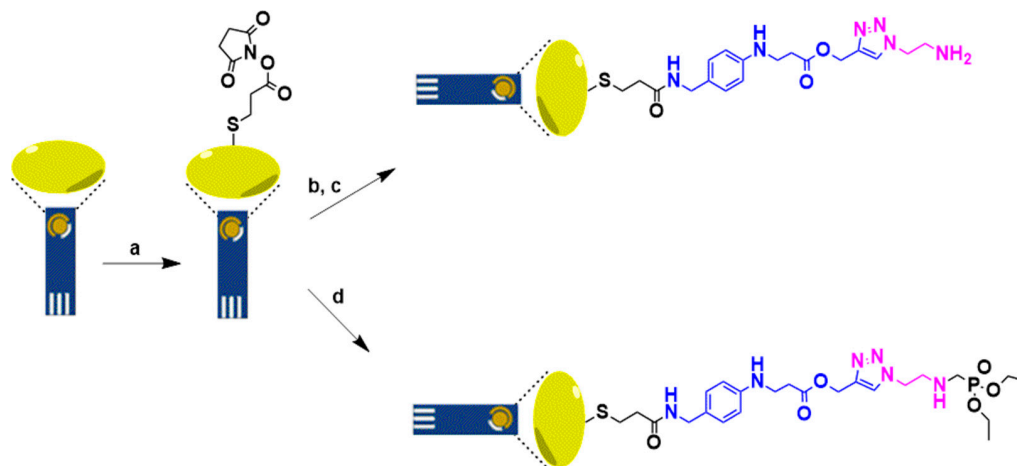


**Figure 1.** Application of the chelating linker on the SPGE. Reagents and conditions: (a) DMSO, 48 h; (b) Piperidine/H<sub>2</sub>O, 1 h; (c) Tr-N, 48 h; (d) Tr-P, 48 h.

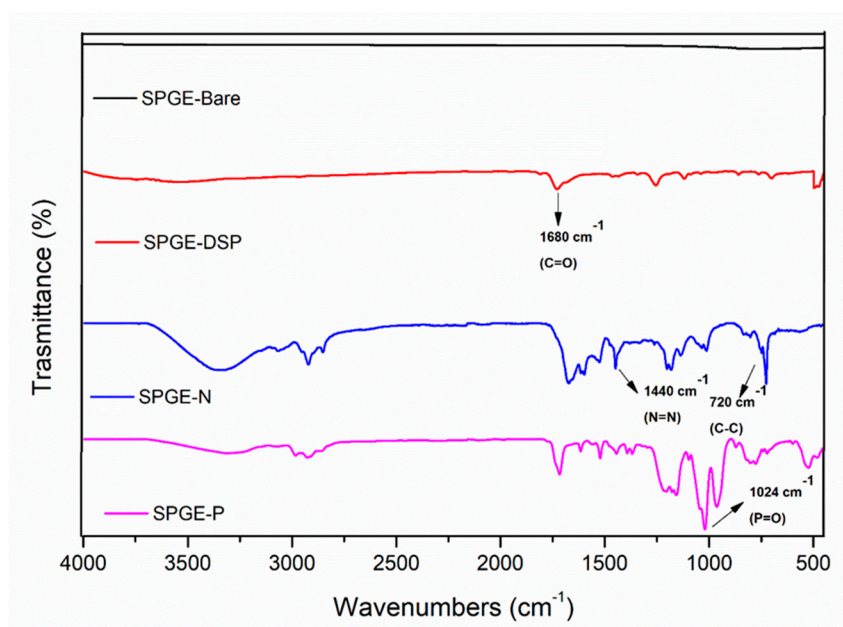


**Figure 2.** ATR-FTIR spectra of SPGE, SPGE-DSP, SPGE-N, and SPGE-P.

### 3.3. Electrochemical Properties of Bare SPGE, SPGE-N, and SPGE-P

The electrochemical characteristics of modified SPGEs were evaluated by CV and EIS and were compared with those obtained from SPGEs (Figure 3). For cyclic voltammetry (Figure 3a), the voltage applied to the working electrode was run from  $-0.3$  V to  $+0.6$  V at a scan rate of  $50$  mV/s in a  $5$  mM solution of  $K_3[Fe(CN)_6]$  in PBS. A pair of redox peaks was recorded, underlining the electron transfer rate at the electrode–electrolyte interface.

These results were also demonstrated by EIS analysis; as shown in Figure 3b, SPGE shows a larger semicircle ( $R_{ct} = 488 \Omega$ ) compared to SPGE-N ( $R_{ct} = 124 \Omega$ ). These values indicate a decrease in the resistance of the modified electrode, greatly improving the ability of the modified sensor (SPGE-N) to perform the oxidation and reduction of the analytes. As for SPGE-P, this shows a larger semicircle than SPGE ( $R_{ct} = 1110 \Omega$ ). The observed differences in RCT values can be rationalized considering the different chemical functionalization of the modified SPGEs. Since the main differences between SPGE-P and SPGE-N is the presence of amino groups (in SPGE-N) or sterically bulky phosphonic groups (in SPGE-P), it is conceivable that the active surface area, where the transfer of electrons takes place, is reduced for the modified electrodes, and, in particular, for SPGE-P,

thus leading to higher RCT values for the modified sensors. Similar responses have also been observed in the literature for SPGE functionalized with consistent organic layers [62].

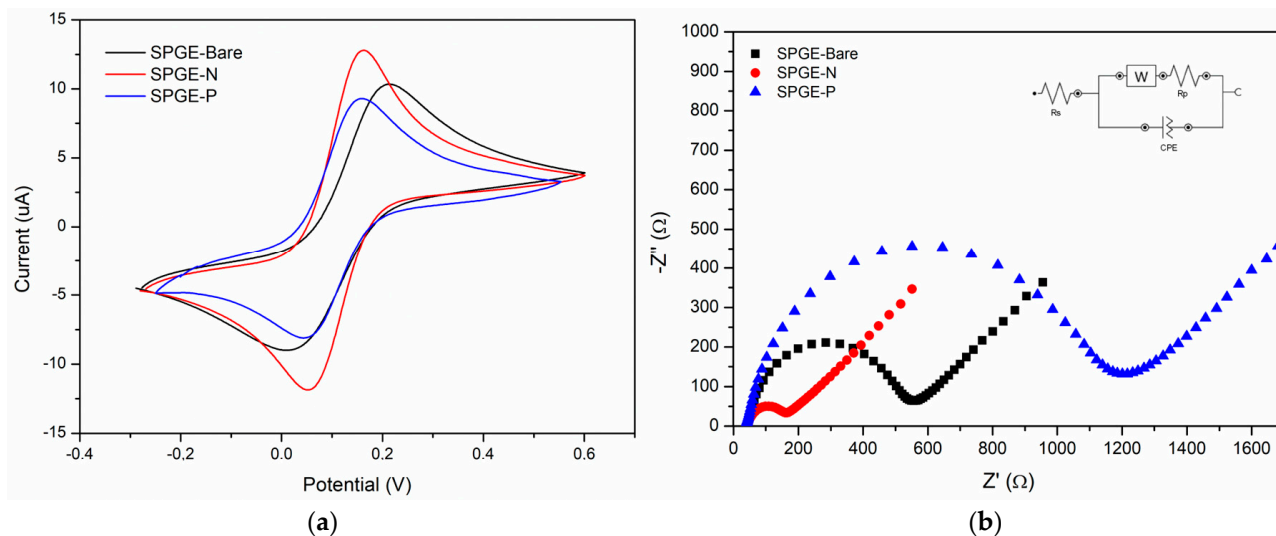


**Figure 3.** (a) Cyclic voltammogram of SPGE-Bare, **SPGE-N**, and **SPGE-P** in 0.01 M PBS (pH 7.4), scan rate 50 mV/s. (b) EIS of SPGE-Bare, **SPGE-N**, and **SPGE-P** in a solution containing 5 mM  $[\text{Fe}(\text{CN})_6]^{3-/4-}$  and 0.1 M KCl with a frequency range from 0.1 Hz to 0.1 MHz.

The determination of electrochemical active area (ECSA) values is essential to obtain a comparison of the performance between different electrodes and can provide useful indications of changes at the electrode interface after modification. Indeed, the observed improvement in the redox peak current values of ligand-based electrodes could be attributed to faster electron transfer kinetics and its higher electroactive surface area. The Randles–Sevcik formula was employed to find out the active surface area of SPGE, **SPGE-N**, and **SPGE-P** using  $\text{K}_4[\text{Fe}(\text{CN})_6]/\text{K}_3[\text{Fe}(\text{CN})_6]$  as the redox probe:

$$I_p = 2.69 \times 10^5 n^{3/2} A D^{1/2} C v^{1/2} \quad (1)$$

where  $I_p$  is the peak current measured at the redox potential,  $n = 1$  is the number of electrons transferred in the redox event,  $A = 0.126 \text{ cm}^2$  is the surface area of the electrode ( $\text{cm}^2$ ),  $D = 7.6 \times 10^{-6} \text{ cm}^2 \text{ s}^{-1}$  is the diffusion coefficient ( $\text{cm}^2 \text{ s}^{-1}$ ),  $C$  is the concentration of the redox probe (ranging from 1 to 10 mM ( $10^{-6}$  to  $10^{-5} \text{ mol cm}^3$ ), and  $v = 0.05$  is the potential scan rate ( $\text{Vs}^{-1}$ ). From the slope of Equation (1), the calculated areas for SPGE-Bare, **SPGE-N**, and **SPGE-P** were found to be 0.0063, 0.0076, and 0.0056  $\text{cm}^2$ , respectively, confirming that the electrode surface had been modified.

The selectivity of the electrodes was assessed by square wave voltammetry, testing them with different analytes, such as  $\text{Ni}^{2+}$ ,  $\text{Cu}^{2+}$ ,  $\text{Cd}^{2+}$ ,  $\text{Pb}^{2+}$ , and  $\text{Hg}^{2+}$ . As shown in Figure 4, a significant response for  $\text{Pb}^{2+}$  is recorded for the **SPGE-N** electrode at the nanomolar concentration, while no significant responses were recorded for  $\text{Ni}^{2+}$ ,  $\text{Cu}^{2+}$ ,  $\text{Cd}^{2+}$ , and  $\text{Hg}^{2+}$  ions. Similarly, a significant response for  $\text{Hg}^{2+}$  were recorded for the **SPGE-P** electrode, while no relevant response was recorded for  $\text{Ni}^{2+}$ ,  $\text{Cu}^{2+}$ ,  $\text{Cd}^{2+}$ , and  $\text{Pb}^{2+}$  ions. These results confirm the specific binding of the synthesized ligands with the target metal ions, guaranteeing the excellent selectivity of the functionalization procedures.

In our previous study, we experimentally evaluated the chelating capacity of this type of system by means of ICP-MS analysis [58,63]. These studies revealed the interesting chelating behavior of the phosphonate system towards the  $\text{Hg}^{2+}$  ion and of the amine system for  $\text{Pb}^{2+}$  ions. Therefore, we detected  $\text{Hg}^{2+}$  and  $\text{Pb}^{2+}$  ions using SPGE and **SPGE-N** electrodes, selective towards  $\text{Pb}^{2+}$  ions, and **SPGE-P**, selective towards  $\text{Hg}^{2+}$  ions, immersed in a 0.1 M acetate buffer solution at pH 4.5 in the concentration range 1–10 nmol, following the SWASV method discussed in Section 2.4.



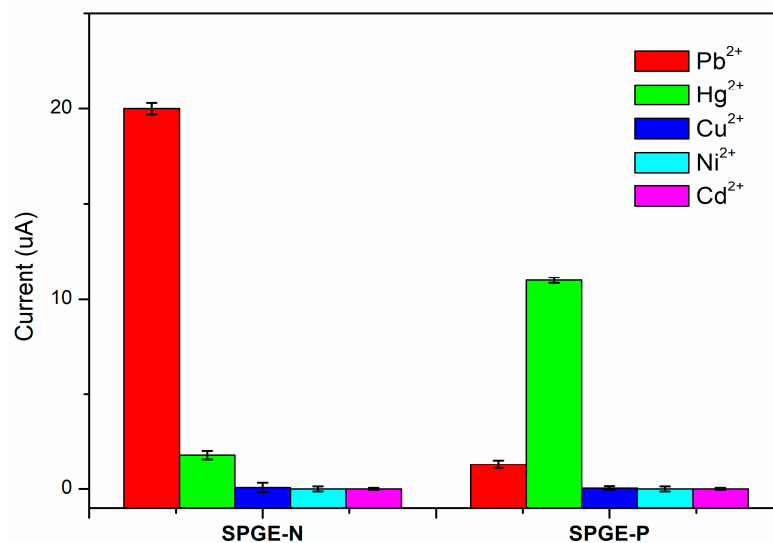


**Figure 4.** Electrochemical response to different heavy metal ions of **SPGE-N** and **SPGE-P**.

Figure 5a shows the square-wave stripping anodic voltammetry (SWASV) analyses with the **SPGE-N** electrode, which were carried out ranging from  $-0.5$  V to  $0.0$  V by adding small volumes of aqueous  $\text{Pb}^{2+}$  solutions (in the concentration range of  $1$ – $10$  nM) into a cell containing a pH 4.5 buffer solution. Preliminary results obtained for **SPGE-N** show a detection capability towards  $\text{Pb}^{2+}$  ions more than 20 times higher than SPGE. Upon the addition of the  $\text{Pb}^{2+}$  solution, the ion stripping peak at  $-0.20$  V can be observed, while Figure 5b shows the corresponding calibration graph recorded in the concentration range of  $1$ – $10$  nmol. Likewise, Figure 5c shows the SWASV analysis performed on the **SPGE-P** electrode, ranging from  $-0.3$  V to  $0.6$  V, by adding aqueous solutions of  $\text{Hg}^{2+}$  ions (concentration range of  $1$ – $10$  nM) in a pH 4.5 buffer solution, which revealed a higher detection capability of  $\text{Hg}^{2+}$  ions of more than 100 times that of bare SPGE (Figure 5c). Upon the addition of the  $\text{Hg}^{2+}$  solution, the ion stripping peak at  $0.20$  V can be observed, while Figure 5d shows the corresponding calibration graph performed in the concentration range of  $1$ – $10$  nmol.

The above results, summarized in Figure 6, show the improved performance of the modified **SPGE-N** and **SPGE-P** electrodes, compared to SPGE, in selectively detecting  $\text{Pb}^{2+}$  and  $\text{Hg}^{2+}$  ions, respectively. In fact, for these ions, there is a marked improvement in the detection capability of over eight times for **SPGE-N** and ten times for **SPGE-P** when compared to the bare electrode.

The modified electrodes show the ability to detect heavy metal ions simultaneously and selectively when they are added at different concentrations, as illustrated in Figure 6. The peak current of the stripping reaction shows a proportional increase with the concentration, establishing a strong linear relationship in the concentration range between  $1$  nM and  $10$  nM for the metal ions under investigation. The ability to detect heavy metal ions at very low concentrations is essential for environmental applications.

The repeatability of the response of the modified electrodes to the addition of heavy metal ions was evaluated by performing five replicate tests in an acetate buffer solution (pH 4.5) with a final concentration of  $10$  nM for each metal. The results obtained and the average standard deviations for the oxidation peaks of SWASV are reported in Figure 7. The results showed that **SPGE-N** and **SPGE-P** have high and good repeatability for the detection of lead and mercury ions, respectively. The relative standard deviations (RSDs) evaluated after five experiments for  $\text{Pb}^{2+}$  and  $\text{Hg}^{2+}$  ions were  $0.29$  and  $0.14$ , respectively.

These RSD values of less than 1% for all tests performed indicate excellent repeatability. The LOD values were evaluated using the following formula:

$$\text{LOD} = 3 \times \left( \frac{SD}{S} \right) \quad (2)$$

where  $SD$  is the standard deviation of three peak currents measured at the lowest concentration (50 ppb) and  $S$  is the slope of the calibration curve. The calculated limits of detection (LOD) were 0.41 nM and 0.035 nM for  $\text{Pb}^{2+}$  and  $\text{Hg}^{2+}$ , respectively. The sensitivity of the sensors, computed as the slope of the calibration curve, were  $5.84 \mu\text{A nM}^{-1} \text{cm}^{-2}$  and  $10 \mu\text{A nM}^{-1} \text{cm}^{-2}$ , respectively, for  $\text{Pb}^{2+}$  and  $\text{Hg}^{2+}$ .

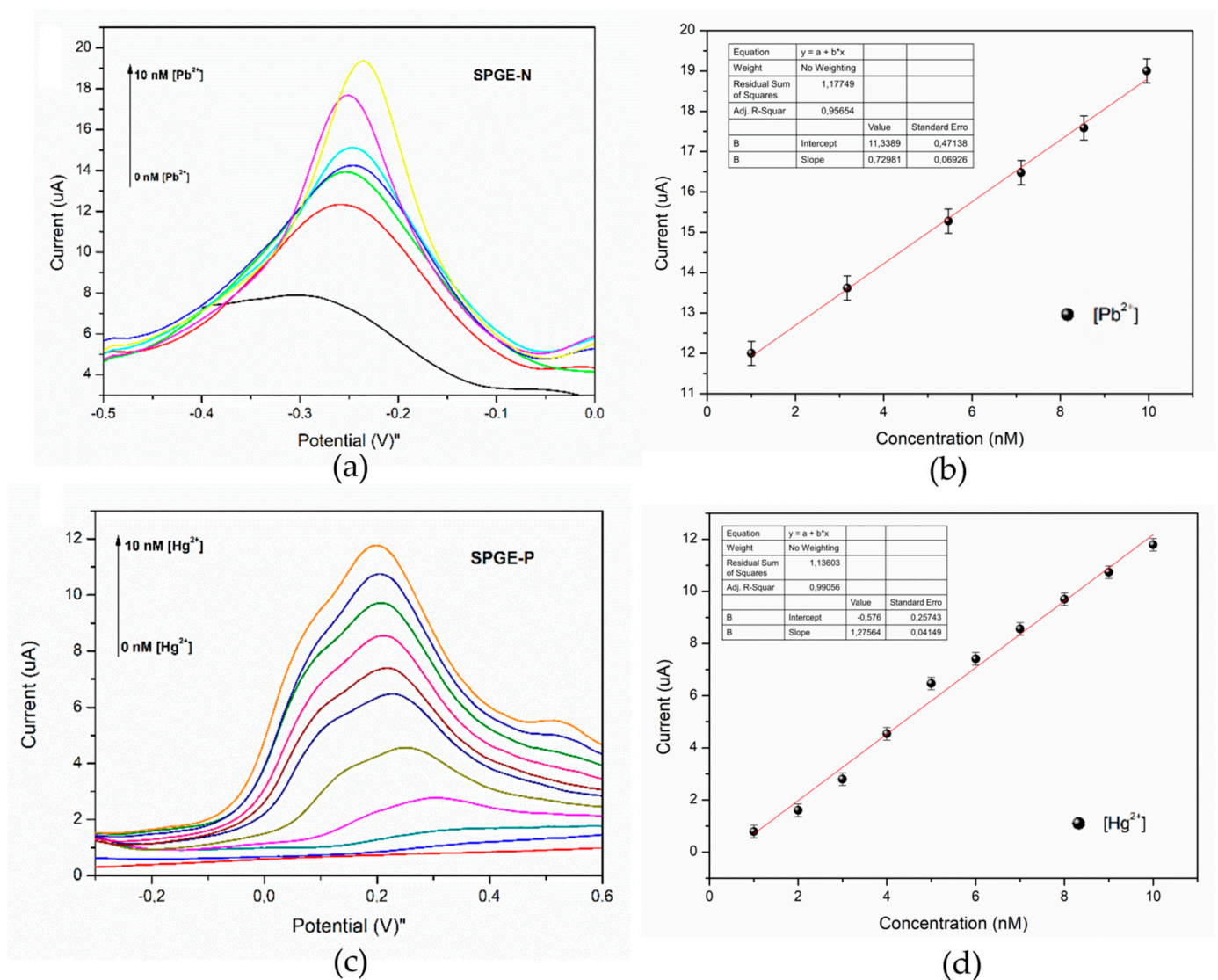


**Figure 5.** (a) SWASV of SPGE-N upon addition of  $\text{Pb}^{2+}$  ions (stripping peak at around  $-0.25 \text{ V}$ ) and (b) calibration graph at ion concentrations of 1–10 nmol. (c) SWASV of SPGE-P upon addition of  $\text{Hg}^{2+}$  ions (stripping peak at around  $+0.2 \text{ V}$ ) and (d) calibration graph at ion concentrations of 1–10 nmol.

It is known that the analytical performance of pure gold thin-film electrodes with regard to heavy metal detection is not very high [64], but this ligand-selective chemical modification showed the potential to overcome this drawback.

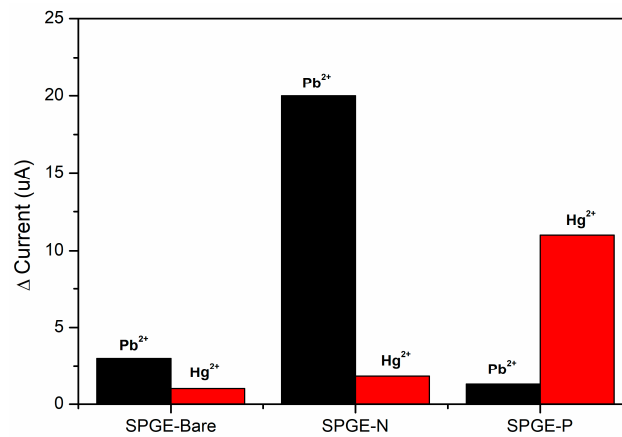


**Figure 6.** Electrochemical behavior of SPGE, SPGE-N, and SPGE-P in response to the presence of 10 nM of  $\text{Pb}^{2+}$  and  $\text{Hg}^{2+}$ .

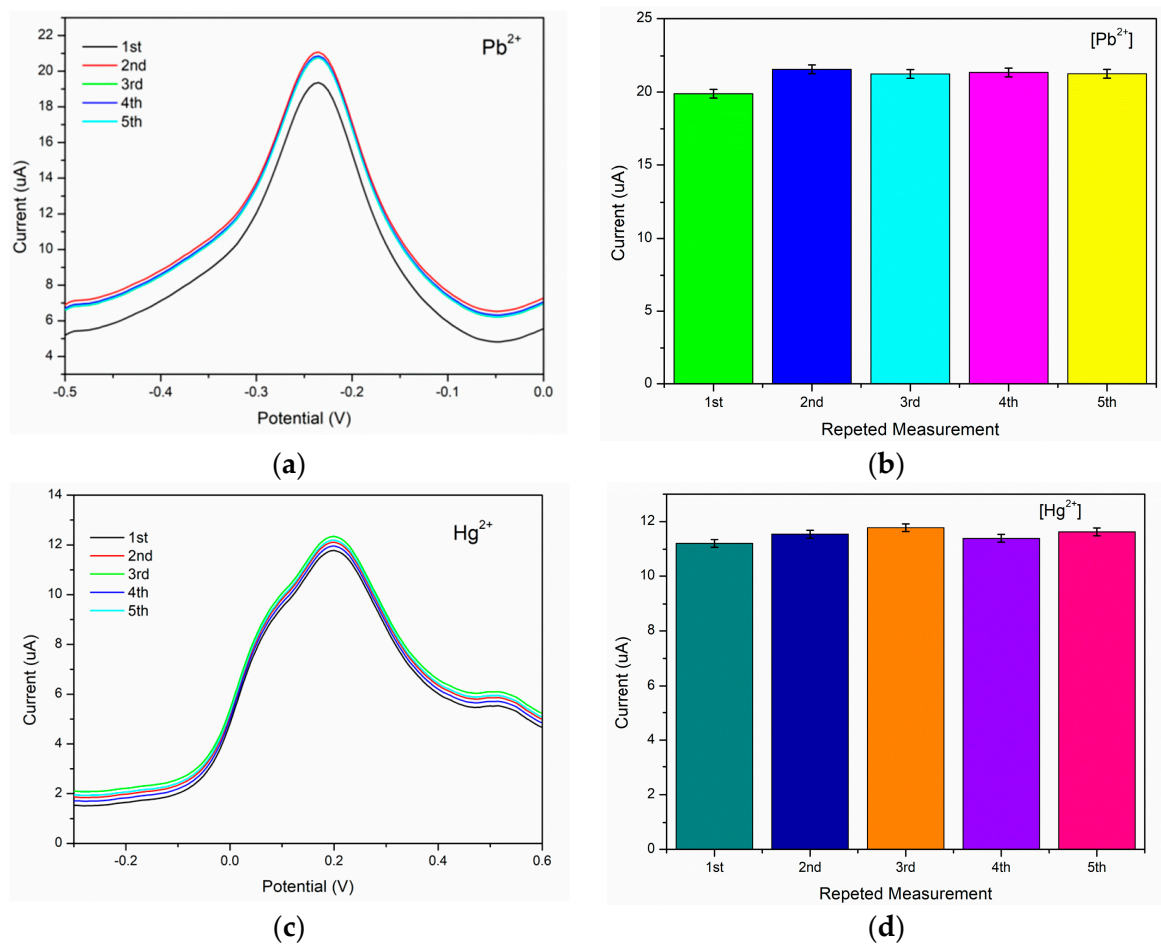


**Figure 7.** (a) Measurement curves of repeatability results obtained after several tests performed with the same SPGE-N sensor at 10 nM; (b) Histograms of repeatability results obtained after several tests with the same SPGE-N sensor at 10 nM; (c) Measurement curves of repeatability results obtained after several tests performed with the same SPGE-P sensor at 10 nM; (d) Histograms of repeatability results obtained after several tests with the same SPGE-N sensor at 10 nM.

The performances of the proposed sensors such as the linear range, sensitivity, and limit of detection were compared with the most recent reports in the literature (Table 1).

**Table 1.** Performance of the modified **SPGE-N** and **SPGE-P** gold electrodes proposed in this study for the detection of  $\text{Pb}^{2+}$  and  $\text{Hg}^{2+}$ , respectively. For comparison, the performances of previous screen-printed gold electrodes for the detection of heavy metal ions are also shown.

Electrodes	LOD (nM)	Linear Range (nM)	Analyte	Technique	Ref.
Screen-printed gold electrode	0.6	10–10,000	$\text{Hg}^{2+}$	CV	[65]
Au-(Cys)PW	4.0	0.01–0.2	$\text{Pb}^{2+}$	SWV	[66]
Screen-printed gold electrode	500	0–50,000	$\text{Pb}^{2+}$	SWASV	[67]
PTO/Au	0.06	0.2–1	$\text{Hg}^{2+}$	DPV	[68]
MCGE	7.1	1.7–9.3	$\text{Pb}^{2+}$	DPSV	[69]
Au-TiO <sub>2</sub> NPs/Chit/gold-modified electrode	1.0	5.0–400.0	$\text{Hg}^{2+}$	DPSV	[70]
<b>SPGE-N</b>	0.41	0–10	$\text{Pb}^{2+}$	SWASV	This work
<b>SPGE-P</b>	0.035	0–10	$\text{Hg}^{2+}$	SWASV	This work

#### 4. Real Samples Analyses

The above-reported tests show that the developed modified platforms are very sensitive for the determination of toxic heavy metal ions at low traces. Therefore, we verified the efficiency of our electrodes in the detection of  $\text{Pb}^{2+}$  and  $\text{Hg}^{2+}$  in irrigation water by adding known amounts of the toxic heavy metal ions here investigated. The amounts used for contamination are below the maximum residue limits (MRLs) for these ions, as proposed by the EU directive. The procedure involved the detection of the two heavy metals analyzed in real water samples, previously diluted with acetate buffer (ratio 1:9, water/acetate buffer). The experiments were repeated three times, and the results obtained indicated that the recommended electrochemical method has the potential to accurately detect heavy metal ions in water samples. When compared to the response obtained in acetate buffer, the responses observed with real samples (Figure 8) confirmed that the sensor is not affected by the effect of the matrix.

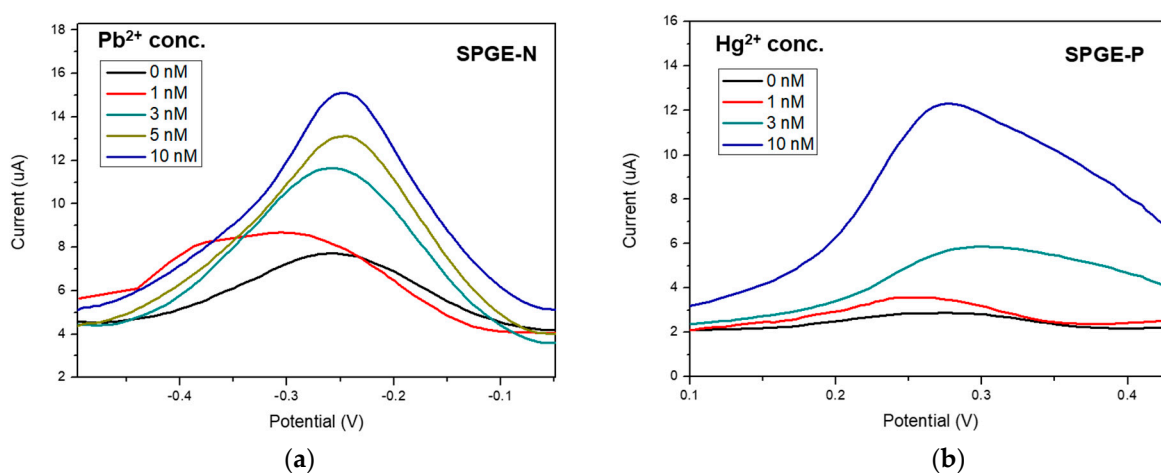


**Figure 8.** (a) SWASV of **SPGE-N** upon the addition of  $\text{Pb}^{2+}$  ions at ion concentrations of 0 and 10 nmol in real sample. (b) SWASV of **SPGE-P** to the addition of  $\text{Hg}^{2+}$  ions at ionic concentrations of 0 and 10 nmol in real sample.

Recovery values were evaluated as follows: Recovery (%) = (nM  $\text{Pb}^{2+}$  or  $\text{Hg}^{2+}$  found/nM  $\text{Pb}^{2+}$  or  $\text{Hg}^{2+}$  expected)  $\times$  100. The recovery values found, as shown in Table 2, were in the range of 96–132.2% for the lead ions on the **SPGE-N** electrode and were between 92.6 and 104.3% for mercury ions on the **SPGE-P** electrode. The experiments were repeated

three times, and high recoveries were obtained for all the heavy metal ions investigated in this study.

**Table 2.** Determination of  $\text{Pb}^{2+}$  or  $\text{Hg}^{2+}$  in a real sample.

Modified Electrodes	Spiked (nM)	Found (nM)	Recovery (%)	RSD (%)
SPGE-N	1 of $\text{Pb}^{2+}$	1.16 of $\text{Pb}^{2+}$	116.0	1.39 ( $n = 3$ )
SPGE-N	3 of $\text{Pb}^{2+}$	2.88 of $\text{Pb}^{2+}$	96.0	1.85 ( $n = 3$ )
SPGE-N	5 of $\text{Pb}^{2+}$	6.61 of $\text{Pb}^{2+}$	132.2	3.31 ( $n = 3$ )
SPGE-N	10 of $\text{Pb}^{2+}$	10.47 of $\text{Pb}^{2+}$	104.7	1.28 ( $n = 3$ )
SPGE-P	1 of $\text{Hg}^{2+}$	0.93 of $\text{Hg}^{2+}$	93.0	1.59 ( $n = 3$ )
SPGE-P	3 of $\text{Hg}^{2+}$	2.78 of $\text{Hg}^{2+}$	92.6	2.11 ( $n = 3$ )
SPGE-P	10 of $\text{Hg}^{2+}$	10.43 of $\text{Hg}^{2+}$	104.3	1.98 ( $n = 3$ )

Furthermore, the stability of the sensors was evaluated by performing tests after storing the sensors for 6 months under ambient conditions. The **SPGE-N** and **SPGE-P** electrodes retained 92.6% and 93.4% of the initial response, thus indicating good long-term stability.

## 5. Conclusions

In this work, commercially available screen-printed gold electrodes have been functionalized via thiol chemistry with organic ligands able to selectively bind  $\text{Hg}^{2+}$  or  $\text{Pb}^{2+}$  ions for the electrochemical determination of these toxic ions in water. Square-wave anodic stripping voltammetry was applied for the electrochemical detection of these ions, either alone or in their mixtures. SWASV analyses revealed a higher detection capability of the functionalized electrodes when compared to bare SPGE. Better selectivity for  $\text{Pb}^{2+}$  ions was recorded for **SPGE-N**, while **SPGE-P** demonstrated detection capability for  $\text{Hg}^{2+}$  ions at very low concentrations (LOD of 0.41 nM for  $\text{Pb}^{2+}$  and 35 pM for  $\text{Hg}^{2+}$ ). The results of this study demonstrated, for the first time, the improved detection ability of SPGEs towards heavy metals after the chemical modification of the work electrode with properly designed sensitive elements. The reported results represent a valuable starting point for the development of electrochemical sensors which are capable of monitoring toxic trace heavy metals in water using simply modified SPEs and anodic stripping voltammetry.

**Supplementary Materials:** The following supporting information can be downloaded at <https://www.mdpi.com/article/10.3390/s24154935/s1>, NMR and elemental analysis data.

**Author Contributions:** Conceptualization, C.C., D.I. and S.V.G.; methodology, C.E., C.C. and G.N.; software, L.L. and S.V.G.; validation, D.I., G.N. and C.C.; formal analysis, C.C. and S.V.G.; investigation, C.C., D.I. and G.N.; resources, G.N.; data curation, C.C., D.I. and S.V.G.; writing—original draft preparation, C.C. and D.I.; writing—review and editing, C.C., D.I. and S.V.G.; visualization, C.E. and L.L.; supervision, G.N.; project administration, C.E.; funding acquisition, G.N. All authors have read and agreed to the published version of the manuscript.

**Funding:** This work has been partially funded by the European Union (Next Generation EU) through the MUR-PNRR project SAMOTHRACE (ECS00000022).

**Institutional Review Board Statement:** Not applicable.

**Informed Consent Statement:** Not applicable.

**Data Availability Statement:** Data are contained within the article.

**Conflicts of Interest:** The authors declare no conflicts of interest.

## References

1. Lu, M.; Deng, Y.; Luo, Y.; Lv, J.; Li, T.; Xu, J.; Chen, S.W.; Wang, J. Graphene Aerogel-Metal-Organic Framework-Based Electrochemical Method for Simultaneous Detection of Multiple Heavy-Metal Ions. *Anal. Chem.* **2019**, *91*, 888–895. [[CrossRef](#)] [[PubMed](#)]
2. Yang, J.; Zhang, Y.; Zhang, L.; Wang, H.; Nie, J.; Qin, Z.; Li, J.; Xiao, W. Analyte-Triggered Autocatalytic Amplification Combined with Gold Nanoparticle Probes for Colorimetric Detection of Heavy-Metal Ions. *Chem. Commun.* **2017**, *53*, 7477–7480. [[CrossRef](#)]
3. Bansod, B.K.; Kumar, T.; Thakur, R.; Rana, S.; Singh, I. A Review on Various Electrochemical Techniques for Heavy Metal Ions Detection with Different Sensing Platforms. *Biosens. Bioelectron.* **2017**, *94*, 443–455. [[CrossRef](#)] [[PubMed](#)]
4. Zhang, Y.N.; Niu, Q.; Gu, X.; Yang, N.; Zhao, G. Recent Progress on Carbon Nanomaterials for the Electrochemical Detection and Removal of Environmental Pollutants. *Nanoscale* **2019**, *11*, 11992–12014. [[CrossRef](#)]
5. Ielo, I.; Giacobello, F.; Castellano, A.; Sfameni, S.; Rando, G.; Plutino, M.R. Development of Antibacterial and Antifouling Innovative and Eco-Sustainable Sol–Gel Based Materials: From Marine Areas Protection to Healthcare Applications. *Gels* **2022**, *8*, 26. [[CrossRef](#)]
6. Zhang, W.; Liu, Q.X.; Guo, Z.H.; Lin, J.S. Practical Application of Aptamer-Based Biosensors in Detection of Low Molecular Weight Pollutants in Water Sources. *Molecules* **2018**, *23*, 344. [[CrossRef](#)] [[PubMed](#)]
7. Veerakumar, P.; Veeramani, V.; Chen, S.M.; Madhu, R.; Liu, S. Bin Palladium Nanoparticle Incorporated Porous Activated Carbon: Electrochemical Detection of Toxic Metal Ions. *ACS Appl. Mater. Interfaces* **2016**, *8*, 1319–1326. [[CrossRef](#)]
8. Moulae, K.; Bressi, V.; Ferlazzo, A.; Iannazzo, D.; Espro, C.; Neri, G. Electrochemical Stripping Determination of Trace Heavy Metals Using Screen-Printed Electrodes as a Versatile Approach toward a Mobile Sensing Platform. In Proceedings of the 2022 IEEE International Workshop on Metrology for the Sea; Learning to Measure Sea Health Parameters (MetroSea), Milazzo, Italy, 3–5 October 2022; pp. 164–167. [[CrossRef](#)]
9. Li, S.S.; Li, W.J.; Jiang, T.J.; Liu, Z.G.; Chen, X.; Cong, H.P.; Liu, J.H.; Huang, Y.Y.; Li, L.N.; Huang, X.J. Iron Oxide with Different Crystal Phases ( $\alpha$ - and  $\gamma$ -Fe<sub>2</sub>O<sub>3</sub>) in Electroanalysis and Ultrasensitive and Selective Detection of Lead(II): An Advancing Approach Using XPS and EXAFS. *Anal. Chem.* **2016**, *88*, 906–914. [[CrossRef](#)]
10. Waheed, A.; Mansha, M.; Ullah, N. Nanomaterials-Based Electrochemical Detection of Heavy Metals in Water: Current Status, Challenges and Future Direction. *TrAC—Trends Anal. Chem.* **2018**, *105*, 37–51. [[CrossRef](#)]
11. Lu, L.; Zhou, L.; Chen, J.; Yan, F.; Liu, J.; Dong, X.; Xi, F.; Chen, P. Nanochannel-Confined Graphene Quantum Dots for Ultrasensitive Electrochemical Analysis of Complex Samples. *ACS Nano* **2018**, *12*, 12673–12681. [[CrossRef](#)]
12. Priya, T.; Dhanalakshmi, N.; Thennarasu, S.; Thinakaran, N. A Novel Voltammetric Sensor for the Simultaneous Detection of Cd<sup>2+</sup> and Pb<sup>2+</sup> Using Graphene Oxide/ $\kappa$ -Carrageenan/L-Cysteine Nanocomposite. *Carbohydr. Polym.* **2018**, *182*, 199–206. [[CrossRef](#)] [[PubMed](#)]
13. Abdulla, M.; Ali, A.; Jamal, R.; Bakri, T.; Wu, W.; Abdiryim, T. Electrochemical Sensor of Double-Thiol Linked PProDOT@Si Composite for Simultaneous Detection of Cd(II), Pb(II), and Hg(II). *Polymers* **2019**, *11*, 815. [[CrossRef](#)] [[PubMed](#)]
14. Cancelliere, R.; Di Tinno, A.; Cataldo, A.; Bellucci, S.; Micheli, L. Powerful Electron-Transfer Screen-Printed Platforms as Biosensing Tools: The Case of Uric Acid Biosensor. *Biosensors* **2022**, *12*, 2. [[CrossRef](#)] [[PubMed](#)]
15. Ramanavicius, S.; Ramanavicius, A. Conducting Polymers in the Design of Biosensors and Biofuel Cells. *Polymers* **2021**, *13*, 49. [[CrossRef](#)] [[PubMed](#)]
16. Miao, P.; Tang, Y.; Wang, L. DNA Modified Fe<sub>3</sub>O<sub>4</sub>@Au Magnetic Nanoparticles as Selective Probes for Simultaneous Detection of Heavy Metal Ions. *ACS Appl. Mater. Interfaces* **2017**, *9*, 3940–3947. [[CrossRef](#)] [[PubMed](#)]
17. Li, Z.; Li, Q.; Jiang, R.; Qin, Y.; Luo, Y.; Li, J.; Kong, W.; Yang, Z.; Huang, C.; Qu, X.; et al. An Electrochemical Sensor Based on a MOF/ZnO Composite for the Highly Sensitive Detection of Cu(I) in River Water Samples. *RSC Adv.* **2022**, *12*, 5062–5071. [[CrossRef](#)] [[PubMed](#)]
18. United States Environmental Protection Agency. *Lead and Copper Rule: A Quick Reference Guide*; United States Environmental Protection Agency: Washington, DC, USA, 2008; Volume 85, pp. 1–2.
19. WHO. *Mercury in Drinking-Water, Background Document for Development of WHO Guidelines for Drinking-Water Quality*; WHO/SDE/WS, WHO/SDE/WSH/05.08/10; WHO: Geneva, Switzerland, 2005.
20. Beitollahi, H.; Tajik, S.; Dourandish, Z.; Zhang, K.; Le, Q.V.; Jang, H.W.; Kim, S.Y.; Shokouhimehr, M. Recent Advances in the Aptamer-Based Electrochemical Biosensors for Detecting Aflatoxin B1 and Its Pertinent Metabolite Aflatoxin M1. *Sensors* **2020**, *20*, 3256. [[CrossRef](#)] [[PubMed](#)]
21. Zounr, R.A.; Tuzen, M.; Deligonul, N.; Khuhawar, M.Y. A Highly Selective and Sensitive Ultrasonic Assisted Dispersive Liquid Phase Microextraction Based on Deep Eutectic Solvent for Determination of Cadmium in Food and Water Samples Prior to Electrothermal Atomic Absorption Spectrometry. *Food Chem.* **2018**, *253*, 277–283. [[CrossRef](#)]
22. Zhang, M.; Zhang, X.; Niu, P.; Shen, T.; Yuan, Y.; Bai, Y.; Wang, Z. On-Site Low-Power Sensing Nodes for Distributed Monitoring of Heavy Metal Ions in Water. *Nanotechnol. Precis. Eng.* **2021**, *4*, 013005. [[CrossRef](#)]
23. Bono, M.S.; Hanhauser, E.B.; Vaishnav, C.; Hart, A.J.; Karnik, R. Iron Oxide Xerogels for Improved Water Quality Monitoring of Arsenic(III) in Resource-Limited Environments via Solid-Phase Extraction, Preservation, Storage, Transportation, and Analysis of Trace Contaminants (SEPSTAT). *Anal. Methods* **2021**, *13*, 2165–2174. [[CrossRef](#)]
24. Jackson, B.; Taylor, V.; Baker, R.A.; Miller, E. Low-Level Mercury Speciation in Freshwaters by Isotope Dilution GC-ICP-MS. *Environ. Sci. Technol.* **2009**, *43*, 2463–2469. [[CrossRef](#)] [[PubMed](#)]

25. Kong, L.; Hu, X.; Peng, X.; Wang, X. Specific H<sub>2</sub>S Release from Thiosulfate Promoted by UV Irradiation for Removal of Arsenic and Heavy Metals from Strongly Acidic Wastewater. *Environ. Sci. Technol.* **2020**, *54*, 14076–14084. [[CrossRef](#)] [[PubMed](#)]
26. Rodríguez Giraldo, Y.; Rodríguez Sánchez, E.; Torres, L.G.; Montenegro, A.C.; Pichimata, M.A. Development of Validation Methods to Determine Cadmium in Cocoa Almond from the Beans by ICP-MS and ICP-OES. *Talanta Open* **2022**, *5*, 100078. [[CrossRef](#)]
27. Weller, A.; Zok, D.; Reinhard, S.; Woche, S.K.; Guggenberger, G.; Steinhäuser, G. Separation of Ultratrace of Radiosilver from Radiocesium for Environmental Nuclear Forensics. *Anal. Chem.* **2020**, *92*, 5249–5257. [[CrossRef](#)]
28. Qian, J.; Gao, X.; Pan, B. Nanoconfinement-Mediated Water Treatment: From Fundamental to Application. *Environ. Sci. Technol.* **2020**, *54*, 8509–8526. [[CrossRef](#)] [[PubMed](#)]
29. Turner, A. Heavy Metals in the Glass and Enamels of Consumer Container Bottles. *Environ. Sci. Technol.* **2019**, *53*, 8398–8404. [[CrossRef](#)]
30. Ullah, H.; Lun, L.; Rashid, A.; Zada, N.; Chen, B.; Shahab, A.; Li, P.; Ali, M.U.; Lin, S.; Wong, M.H. *A Critical Analysis of Sources, Pollution, and Remediation of Selenium, an Emerging Contaminant*; Springer: Amsterdam, The Netherlands, 2022; ISBN 0123456789.
31. Qu, L.; Ren, X.; Fan, D.; Kuang, X.; Sun, X.; Wang, B.; Wei, Q.; Ju, H. Split-Type Electrochemical Immunoassay System Triggering Ascorbic Acid-Mediated Signal Magnification Based on a Controlled-Release Strategy. *ACS Appl. Mater. Interfaces* **2021**, *13*, 29179–29186. [[CrossRef](#)]
32. Umegaki, I.; Higuchi, Y.; Kondo, Y.; Ninomiya, K.; Takeshita, S.; Tampo, M.; Nakano, H.; Oka, H.; Sugiyama, J.; Kubo, M.K.; et al. Nondestructive High-Sensitivity Detections of Metallic Lithium Deposited on a Battery Anode Using Muonic X-Rays. *Anal. Chem.* **2020**, *92*, 8194–8200. [[CrossRef](#)]
33. Tiihonen, T.E.; Nissinen, T.J.; Turhanen, P.A.; Vepsäläinen, J.J.; Riikonen, J.; Lehto, V.P. Real-Time On-Site Multielement Analysis of Environmental Waters with a Portable X-Ray Fluorescence (PXRF) System. *Anal. Chem.* **2022**, *94*, 11739–11744. [[CrossRef](#)]
34. Gao, K.; Zhang, Z.; Ma, L.; Chen, L.; Chen, X.; Zhang, Y.; Zhang, M. Reversible Supramolecular Adhesives Formed by Metallacycle-Crosslinked Polymer Networks via Amino-yne Click Reaction. *Giant* **2020**, *4*, 100034. [[CrossRef](#)]
35. Yang, L.; Sun, X.; Wei, D.; Ju, H.; Du, Y.; Ma, H.; Wei, Q. Aggregation-Induced Electrochemiluminescence Bioconjugates of Apoferritin-Encapsulated Iridium(III) Complexes for Biosensing Application. *Anal. Chem.* **2021**, *93*, 1553–1560. [[CrossRef](#)] [[PubMed](#)]
36. Wu, C.; Sun, D.X.; Su, M.G.; Yin, Y.P.; Han, W.W.; Lu, Q.F.; Dong, C.Z. Quantitative Analysis of Pb in Soil Samples by Laser-Induced Breakdown Spectroscopy with a Simplified Standard Addition Method. *J. Anal. At. Spectrom.* **2019**, *34*, 1478–1484. [[CrossRef](#)]
37. Hong, A.; Tang, Q.; Khan, A.U.; Miao, M.; Xu, Z.; Dang, F.; Liu, Q.; Wang, Y.; Lin, D.; Filser, J.; et al. Identification and Speciation of Nanoscale Silver in Complex Solid Matrices by Sequential Extraction Coupled with Inductively Coupled Plasma Optical Emission Spectrometry. *Anal. Chem.* **2021**, *93*, 1962–1968. [[CrossRef](#)]
38. Gu, W.; Wang, X.; Wen, J.; Cao, S.; Jiao, L.; Wu, Y.; Wei, X.; Zheng, L.; Hu, L.; Zhang, L.; et al. Modulating Oxygen Reduction Behaviors on Nickel Single-Atom Catalysts to Probe the Electrochemiluminescence Mechanism at the Atomic Level. *Anal. Chem.* **2021**, *93*, 8663–8670. [[CrossRef](#)] [[PubMed](#)]
39. Zhao, D.; Guo, X.; Wang, T.; Alvarez, N.; Shanov, V.N.; Heineman, W.R. Simultaneous Detection of Heavy Metals by Anodic Stripping Voltammetry Using Carbon Nanotube Thread. *Electroanalysis* **2014**, *26*, 488–496. [[CrossRef](#)]
40. Ding, Q.; Cao, L.; Liu, M.; Lin, H.; Yang, D.P. Au Nanoparticle-Loaded Eggshell for Electrochemical Detection of Nitrite. *RSC Adv.* **2021**, *11*, 4112–4117. [[CrossRef](#)] [[PubMed](#)]
41. Iannazzo, D.; Espro, C.; Ferlazzo, A.; Celesti, C.; Branca, C.; Neri, G. Electrochemical and Fluorescent Properties of Crown Ether Functionalized Graphene Quantum Dots for Potassium and Sodium Ions Detection. *Nanomaterials* **2021**, *11*, 2897. [[CrossRef](#)] [[PubMed](#)]
42. Ramachandran, R.; Chen, T.-W.; Chen, S.-M.; Baskar, T.; Kannan, R.; Elumalai, P.; Raja, P.; Jeyapragasam, T.; Dinakaran, K.; Gnana kumar, G.p. A Review of the Advanced Developments of Electrochemical Sensors for the Detection of Toxic and Bioactive Molecules. *Inorg. Chem. Front.* **2019**, *6*, 3418–3439. [[CrossRef](#)]
43. Abid, K.; Iannazzo, D.; Celesti, C.; Khaskhoussi, A.; Foti, A.; Maalej, R.; Gucciardi, P.G.; Neri, G. A Novel 2D-GO@WS<sub>2</sub> Electrochemical Platform for the Determination of Thiram Fungicide. *J. Environ. Sci.* **2022**, *136*, 226–236. [[CrossRef](#)] [[PubMed](#)]
44. Polykretis, P.; Matteini, P.; Iannazzo, D.; Maalej, R. A Study of Screen-Printed Electrodes Modified with MoSe<sub>2</sub> and AuNPs-MoSe<sub>2</sub> Nanosheets for Dopamine Sensing. *Electrochim. Acta* **2023**, *475*, 143371. [[CrossRef](#)]
45. Michenzi, C.; Espro, C.; Bressi, V.; Celesti, C.; Vetica, F.; Salvitti, C.; Chiarotto, I. Electrochemical Bottom-up Synthesis of Biomass-Derived Carbon Dots for Promoting Knoevenagel Condensation. *Mol. Catal.* **2023**, *544*, 113182. [[CrossRef](#)]
46. Ferlazzo, A.; Celesti, C.; Iannazzo, D.; Ampelli, C.; Giusi, D.; Costantino, V.; Neri, G. Functionalization of Carbon Nanofibers with an Aromatic Diamine: Toward a Simple Electrochemical-Based Sensing Platform for the Selective Sensing of Glucose. *ACS Omega* **2024**, *9*, 27085–27092. [[CrossRef](#)] [[PubMed](#)]
47. Wang, Y.; Wang, L.; Huang, W.; Zhang, T.; Hu, X.; Perman, J.A.; Ma, S. A Metal-Organic Framework and Conducting Polymer Based Electrochemical Sensor for High Performance Cadmium Ion Detection. *J. Mater. Chem. A* **2017**, *5*, 8385–8393. [[CrossRef](#)]
48. Rabiee, N.; Ahmadi, S.; Akhavan, O.; Luque, R. Silver and Gold Nanoparticles for Antimicrobial Purposes against Multi-Drug Resistance Bacteria. *Materials* **2022**, *15*, 1799. [[CrossRef](#)] [[PubMed](#)]

49. Kjeldstad, T.; Thogersen, A.; Stange, M.; Azarov, A.; Monakhov, E.; Galeckas, A. Monitoring Selective Etching of Self-Assembled Nanostructured a-Si:Al Films. *Nanotechnology* **2019**, *30*, 135601. [[CrossRef](#)] [[PubMed](#)]
50. WU, Q.; BI, H.M.; HAN, X.J. Research Progress of Electrochemical Detection of Heavy Metal Ions. *Chin. J. Anal. Chem.* **2021**, *49*, 330–340. [[CrossRef](#)]
51. Singh, S.; Wang, J.; Cinti, S. Review—An Overview on Recent Progress in Screen-Printed Electroanalytical (Bio)Sensors. *ECS Sens. Plus* **2022**, *1*, 023401. [[CrossRef](#)]
52. Kasera, N.; Kolar, P.; Hall, S.G. Nitrogen-Doped Biochars as Adsorbents for Mitigation of Heavy Metals and Organics from Water: A Review. *Biochar* **2022**, *4*, 17. [[CrossRef](#)]
53. García-Miranda Ferrari, A.; Rowley-Neale, S.J.; Banks, C.E. Screen-Printed Electrodes: Transitioning the Laboratory in-to-the Field. *Talanta Open* **2021**, *3*, 100032. [[CrossRef](#)]
54. Iannazzo, D.; Celesti, C.; Espro, C.; Ferlazzo, A.; Giofrè, S.V.; Scuderi, M.; Scalese, S.; Gabriele, B.; Mancuso, R.; Zicarelli, I.; et al. Orange-Peel-Derived Nanobiochar for Targeted Cancer Therapy. *Pharmaceutics* **2022**, *14*, 2249. [[CrossRef](#)]
55. Bressi, V.; Celesti, C.; Ferlazzo, A.; Len, T.; Moulæe, K.; Neri, G.; Luque, R.; Espro, C. Waste-Derived Carbon Nanodots for Fluorimetric and Simultaneous Electrochemical Detection of Heavy Metals in Water. *Environ. Sci. Nano* **2024**, *13*, 1245–1258. [[CrossRef](#)]
56. Zamani, M.; Yang, V.; Maziashvili, L.; Fan, G.; Klapperich, C.M.; Furst, A.L. Surface Requirements for Optimal Biosensing with Disposable Gold Electrodes. *ACS Meas. Sci. Au* **2022**, *2*, 91–95. [[CrossRef](#)]
57. Paimard, G.; Ghasali, E.; Baeza, M. Screen-Printed Electrodes: Fabrication, Modification, and Biosensing Applications. *Chemosensors* **2023**, *11*, 113. [[CrossRef](#)]
58. Iannazzo, D.; Pistone, A.; Zicarelli, I.; Espro, C.; Galvagno, S.; Giofrè, S.V.; Romeo, R.; Cicero, N.; Bua, G.D.; Lanza, G.; et al. Removal of Heavy Metal Ions from Wastewaters Using Dendrimer-Functionalized Multi-Walled Carbon Nanotubes. *Environ. Sci. Pollut. Res.* **2017**, *24*, 14735–14747. [[CrossRef](#)] [[PubMed](#)]
59. Sawan, S.; Maalouf, R.; Errachid, A.; Jaffrezic-Renault, N. Metal and Metal Oxide Nanoparticles in the Voltammetric Detection of Heavy Metals: A Review. *TrAC—Trends Anal. Chem.* **2020**, *131*, 116014. [[CrossRef](#)]
60. Romeo, R.; Giofrè, S.V.; Carnovale, C.; Chiacchio, M.A.; Campisi, A.; Mancuso, R.; Cirmi, S.; Navarra, M. Synthesis and Biological Activity of Triazole-Appended N,O-Nucleosides. *Eur. J. Org. Chem.* **2014**, *2014*, 5442–5447. [[CrossRef](#)]
61. Sánchez-Paniagua, M.; Palenzuela-Batista, S.; Manzanares-Palenzuela, C.L.; López-Ruiz, B. Electrochemical Genosensor for Klotho Detection Based on Aliphatic and Aromatic Thiols Self-Assembled Monolayers. *Talanta* **2020**, *212*, 120735. [[CrossRef](#)] [[PubMed](#)]
62. Singhal, C.; Khanuja, M.; Chaudhary, N.; Pundir, C.S.; Narang, J. Detection of Chikungunya Virus DNA Using Two-Dimensional MoS<sub>2</sub> Nanosheets Based Disposable Biosensor. *Sci. Rep.* **2018**, *8*, 7734. [[CrossRef](#)]
63. Giofrè, S.V.; Romeo, R.; Carnovale, C.; Mancuso, R.; Cirmi, S.; Navarra, M.; Garozzo, A.; Chiacchio, M.A. Synthesis and Biological Properties of 5-(1H-1,2,3-Triazol-4-Yl)Isoxazolidines: A New Class of C-Nucleosides. *Molecules* **2015**, *20*, 5260–5275. [[CrossRef](#)]
64. Hou, X.; Xiong, B.; Wang, Y.; Wang, L.; Wang, H. Determination of Trace Lead and Cadmium in Decorative Material Using Disposable Screen-Printed Electrode Electrically Modified with Reduced Graphene Oxide/L-cysteine/Bi-film. *Sensors* **2020**, *20*, 1322. [[CrossRef](#)]
65. Niu, X.; Ding, Y.; Chen, C.; Zhao, H.; Lan, M. A Novel Electrochemical Biosensor for Hg<sup>2+</sup> Determination Based on Hg<sup>2+</sup>-Induced DNA Hybridization. *Sens. Actuators B Chem.* **2011**, *158*, 383–387. [[CrossRef](#)]
66. Dianat, S.; Hatefi-Mehrjardi, A.; Mahmoodzadeh, K.; Kakhki, S. Electrocatalytic Determination of Cd<sup>2+</sup> and Pb<sup>2+</sup> Using an L-Cysteine Tungstophosphate Self-Assembled Monolayer on a Polycrystalline Gold Electrode. *New J. Chem.* **2019**, *43*, 14417–14425. [[CrossRef](#)]
67. Laschi, S.; Palchetti, I.; Mascini, M. Gold-Based Screen-Printed Sensor for Detection of Trace Lead. *Sens. Actuators B Chem.* **2006**, *114*, 460–465. [[CrossRef](#)]
68. Wu, J.; Li, L.; Shen, B.; Cheng, G.; He, P.; Fang, Y. Polythymine Oligonucleotide-Modified Gold Electrode for Voltammetric Determination of Mercury(II) in Aqueous Solution. *Electroanalysis* **2010**, *22*, 479–482. [[CrossRef](#)]
69. Li, W.; Jin, G.; Chen, H.; Kong, J. Highly Sensitive and Reproducible Cyclodextrin-Modified Gold Electrodes for Probing Trace Lead in Blood. *Talanta* **2009**, *78*, 717–722. [[CrossRef](#)]
70. Zhou, L.; Xiong, W.; Liu, S. Preparation of a Gold Electrode Modified with Au–TiO<sub>2</sub> Nanoparticles as an Electrochemical Sensor for the Detection of Mercury(II) Ions. *J. Mater. Sci.* **2014**, *50*, 769–776. [[CrossRef](#)]

**Disclaimer/Publisher’s Note:** The statements, opinions and data contained in all publications are solely those of the individual author(s) and contributor(s) and not of MDPI and/or the editor(s). MDPI and/or the editor(s) disclaim responsibility for any injury to people or property resulting from any ideas, methods, instructions or products referred to in the content.